Sample size effects for Lévy flight of photons in atomic vapors

A. S. M. Macedo ©, J. P. Lopez ©, and T. Passerat de Silans ©*

Departamento de Física, CCEN, Universidade Federal da Paraíba, Caixa Postal 5008, 58051-900 João Pessoa, Paraíba, Brazil

Lévy flight superdiffusion consists of random walks characterized by very long jumps that dominate the transport. However, the finite size of real samples introduces truncation of long jumps and modifies the transport properties. We measure typical Levy flight parameters for photon diffusion in atomic vapor characterized by a Voigt absorption profile. We observe the change of Lévy parameter as a function of truncation length. We associate this variation with size-dependent contributions from different spectral regions of the emission profile with the Doppler core dominating the transport for thin samples and Lorentz wings for thick samples. Monte Carlo simulations are implemented to support the interpretation of results.

I. INTRODUCTION

Lévy flights are a typical random transport in which the particle has a non-negligible probability of moving a step of large length. Those large steps, although rare, rule the transport characteristics, for instance, with mean-square displacement growing faster than linearly in time [1–5]. The possibility of large steps can be mapped in a step-size distribution decaying asymptotically as $P(l) \sim l^{-1-\alpha}$. For $\alpha > 2$ the probability of large steps is very rare and the random walk is a normal diffusion described by the central limit theorem [5]. For $0 < \alpha < 2$ the variance of the step-size distribution diverges, the central limit theorem is not valid anymore, and the random walk is called a Lévy flight. For $0 < \alpha < 1$ even the mean step length $\bar{l}$ diverges and the transport is known as quasiballistic [6].

Lévy flight is encountered in a large variety of systems including turbulence [7], solar light transmitted by cloudy skies [8], charged particle transport in solar wind [6], economy [9,10], displacement of cells [11], displacement of animals [12–14], human travel [15–17], and spread of diseases [18–21]. Information from the random walk mechanism can be obtained from measurable parameters such as sample transmission, mean-square displacement, first time passage, and survival time. The finite size of real samples introduces a cutoff of large steps [1] which may result in size-dependent measured parameters that characterize the superdiffusion [5,22]. Controllable laboratory systems for investigating truncation effects in superdiffusion are of interest and optical devices are good candidates as they allow for repeatability, a large statistics of photons, and the control of parameters. For instance, the effects of quenched [23–25] and annealed [26,27] disorder, the fractal dimension of the random walk [28], and the finite size of system [28] were studied for the Lévy flight of photons in engineered media known as Lévy glasses [3,29] and in atomic vapor [4,26,27,30].

Photons diffuse in resonant media by successive absorption and spontaneous emission, known as radiation trapping, with long jumps being recognized as playing a role in the light transport for a long time [31]. Those long jumps originate in the emission of the photons at the wings of the absorption profile [32]. The Lévy parameter α was measured to be $\alpha \approx 1$ for hot alkali-metal vapor with a Doppler absorption profile [4,26,30] and $\alpha = 0.5$ for a Rb vapor broadened with 50 Torr of He gas [27] with a Lorentz absorption profile. Both results for Doppler and Lorentz profile are consistent with theoretical predictions in the limit of complete frequency redistribution (CFR) [32].

The absorption profiles of alkali-metal vapor are actually Voigt profiles, the convolution of Lorentz and Doppler curves [33,34]. For infinite vapor with a Voigt absorption profile the Lévy flight has the parameter $\alpha = 0.5$ since large steps associated with emission at large detuning at the Lorentz wing dominate the transport [32]. However, truncation makes those large steps inaccessible. The aim of this work is to measure the change in Lévy parameter α for a vapor with a Voigt profile as a function of the system size; in particular, a crossover between Doppler and Lorentz expected α values is obtained.

II. STEP-SIZE DISTRIBUTION

After the photon absorption, the atom remains a typical time τ in the excited state corresponding to the level lifetime. Then it decays spontaneously, emitting a photon that will travel a distance l before being absorbed by another atom, with the travel time being negligible for typical laboratory sample sizes. For the CFR regime the step-size distribution is [32,35]

$$P(r) = \int_{-\infty}^{\infty} \Phi^2(x) e^{-\Phi(x)r} dx, \qquad (1)$$

where $\Phi(x)$ is the vapor absorption profile normalized such that $\int_{-\infty}^{\infty} \Phi(x) dx = 1$ and $x = \delta/\Gamma_D$ is a normalized detuning, with δ the frequency detuning and $\Gamma_D = \frac{u}{\lambda}$ the Doppler half-width at $1/e$ maximum; here λ is the transition wavelength and
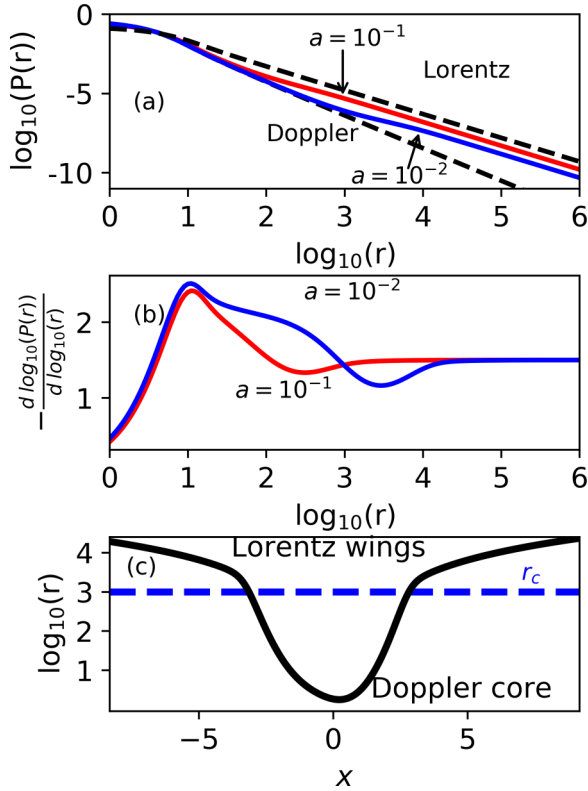
*thierry@otica.ufpb.br

FIG. 1. (a) Step-size probability distribution $P(r)$ calculated from Eq. (1) for Voigt absorption profiles with the parameters $a = 10^{-2}$ (blue line) and $a = 10^{-1}$ (red line). The $P(r)$ are also shown for Doppler and Lorentz absorption profiles as dashed lines. (b) Calculated $-\frac{d \log_{10}[P(r)]}{d \log(r)}$ for $P(r)$ for Voigt absorption profiles with the parameters $a = 10^{-2}$ (blue line) and $a = 10^{-1}$ (red line). (c) Mean absorption length for a photon emitted with detuning x for a Voigt profile with $a = 10^{-2}$. The opacity for crossover between Doppler and Lorentz regimes is represented by the blue dashed line at $r_c \sim 10^3$.

u is the most probable atomic speed. In addition, $r = \frac{l}{l_0} \frac{1}{\Phi(0)}$ is the opacity, a dimensionless parameter related to the ratio between step length l and mean absorption length at line center l_0 [36]. The absorption profile for an atomic vapor at moderate densities is a Voigt profile

$$\Phi(x) = \frac{a}{\pi^{3/2}} \int_{-\infty}^{\infty} e^{-y^2}/[a^2 + (x - y)^2] dy, \qquad (2)$$

where $y = v/u$, v is the velocity component parallel to the photon, and $a = \frac{\Gamma}{2\Gamma_D}$ is the Voigt parameter defined as the ratio of the homogeneous (Γ) to the Doppler (Γ_D) width.

We show in Fig. 1(a) the calculated step length distribution for Voigt profiles with different a parameters as well as for Doppler and Lorentz profiles (dashed lines). A clear crossover is observed from the Doppler to the Lorentz regime at $r_c \sim 10^3$ for a typical value of $a = 10^{-2}$ for alkali-metal vapor (for alkali-metal vapor at tens of degrees Celsius, $\Gamma \sim 5$ MHz and $\Gamma_D \sim 300$ MHz [34]). Writing the step-size distribution as $P(r) \sim r^{-1-\alpha(r)}$, we can access the expected size dependence of $1 + \alpha(r)$ by plotting $-\frac{d}{d \log_{10}(r)} \log_{10}[P(r)]$ as shown in Fig. 1(b). For $a = 10^{-2}$ a value of $\alpha \approx 1.1$ is expected

around $r \sim 10^2$ [32], typical for the Doppler emission profile, and a convergence to $\alpha = 0.5$ corresponding to Lorentz wings is expected for $r > 10^4$. In Fig. 1(c) we show the mean absorption distance for a photon emitted at normalized detuning x. Photons emitted in the Doppler core of the Voigt profile are responsible for steps sizes below r_c, while photons emitted in Lorentzian wings cause steps larger than r_c. The finiteness of real samples introduces a cutoff r_S of step sizes [1]. For sample dimensions below the crossover limit ($r_S < r_c$) only photons emitted in the Doppler core of the Voigt profile are scattered inside the sample, resulting in a Lévy flight with $\alpha \approx 1$, as was measured in [4,26,30]. To reveal Lorentz wing contributions, samples larger than r_c must be considered. Our experimental setup allows us to vary r_S across r_c and to observe a change in the Lévy parameter as a function of truncation length.

III. EXPERIMENT

A. Setup

To determine the Lévy parameter we measure diffuse transmission as a function of the sample opacity. Our system consists of a heated cesium vapor illuminated by a low-power cw semiconductor laser with an external grating cavity, resonant with the D_2 line of Cs ($\lambda = 852$ nm). The sample opacity is varied through the vapor's atomic density, which affects the line center absorption length l_0. After a random walk inside the vapor, photons transmitted through output windows are collected by a lens, at a distance of 30 cm, into a detector at an angle $\theta = 15°$ relative to the incident beam direction [see Fig. 2(a)]. A relatively large angle for diffusive transmission measurement is used to minimize the scattered light from coherent transmission detection optics. Larger angles were tested with the same results. In Fig. 2(b) we show examples of diffuse transmission spectra when the laser is scanned around the $6S_{1/2}(F = 4) \rightarrow 6P_{3/2}(F' = 3, 4, 5)$ transition with a clear lowering of the detected-signal amplitude around the line center for increasing opacities. We can extract the Lévy α parameter from the scales of the diffuse transmission as a function of sample opacity for a superdiffusive transport [26,27,37,38]:

$$T_D \propto r^{-\alpha/2}. \qquad (3)$$

We use a cylindrical cell with radius $R = 1.25$ cm and thickness $L = 3$ cm. The cell is involved with ovens heating separately the cell body and a reservoir containing liquid Cs. The reservoir temperature T_R controls the Cs pressure in the probed region and the windows' temperatures T_W are kept at least $\sim 20 °$C higher than T_R to avoid Cs condensation on them. Opacity of the sample is determined from the fit of coherent transmission of the laser beam (see the Appendixes for details) and is varied through the vapor density by changing the reservoir temperature. The opacity is varied over a range from $r = 8$ to $r = 1.5 \times 10^5$ corresponding to density variation from $N = 3 \times 10^{10}$ atoms/cm^3 to $N = 6 \times 10^{14}$ atoms/cm^3. To obtain this range of density the cell temperatures are varied from $T_R = 35 °$C and $T_W = 80 °$C, with a corresponding Doppler width of $\Gamma_D \sim 250$ MHz for $r = 8$, to $T_R = 170 °$C
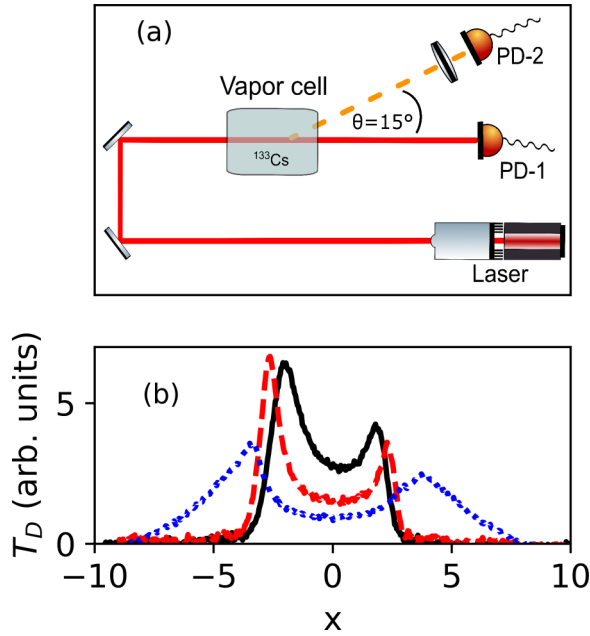
FIG. 2. (a) Scheme of the experimental setup. Here PD-1 and PD-2 are photodetectors: PD-1 is used to measured coherent transmission in the beam direction and PD-2 is used to measure diffuse transmission at an angle of 15° from beam direction. (b) Observed diffuse transmission spectra for three different samples opacities: $r = 25$ (black solid line), $r = 200$ (red dashed line), and $r = 3500$ (blue dotted line). Those opacities correspond to atomic densities (reservoir temperatures) of $N = 9.4 \times 10^{10}$ atoms/cm³ ($T_R = 45\,°C$), $N \approx 7.3 \times 10^{11}$ atoms/cm³ ($T_R = 65\,°C$), and $N = 1.2 \times 10^{13}$ atoms/cm³ ($T_R = 110\,°C$), respectively.

and $T_W = 200\,°C$, with a corresponding Doppler width of $\Gamma_D \sim 285$ MHz for $r = 1.5 \times 10^5$.

The incident beam has a diameter of 1.25 mm, which is much smaller than the cell radius. For low opacity ($r \sim$ 8–200) we use an incident power of $\sim 30\ \mu W$, corresponding to 1.5 times the saturation intensity of the D_2 transition. The penetration depth l_I of the beam is much smaller than the cell thickness ($l_I \sim 10$ mm for $r = 8$ and $l_I \sim 0.5$ mm for $r = 200$). For higher opacities [$r \sim 430$–(1.5×10^5)] we have to increase the incident power to have a good signal-to-noise ratio in the diffusive transmission. We use an incident power of $\sim 300\ \mu W$, corresponding to 15 times the saturation intensity, and penetration depth of $l_I \sim 0.5$ mm for $r = 430$ to $l_I \sim 2\ \mu m$ for $r = 1.5 \times 10^5$.

B. Experimental results

The main result of the article is shown in Fig. 3, where we plot diffuse transmission as a function of sample opacity. We fit experimental data with Eq. (3) and obtain $\alpha = 1.2 \pm 0.2$ for low opacities (first three points), which is consistent with the expected value for a Doppler absorption profile. For higher opacities (last seven points) we obtain $\alpha = 0.50 \pm 0.04$, which is consistent with the expected value for a Lorentz absorption profile.

The points of Fig. 3 are the diffuse transmission amplitude at the transition frequency from the ground state $F = 4$ to the $F' = 4$–5 crossover [denoted by $x = 0$ in Fig. 2(b)]; similar
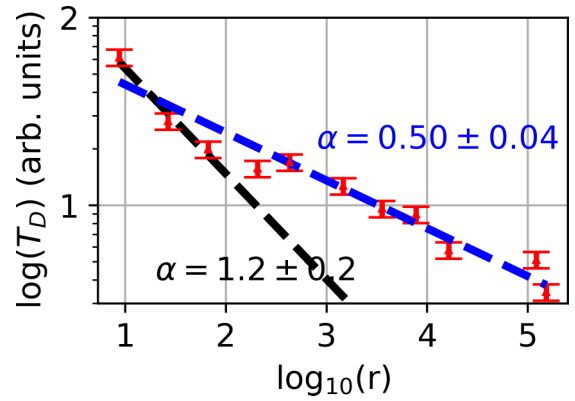

FIG. 3. Measured diffuse transmission as a function of sample opacity. Dashed lines are fits to the experimental data using Eq. (3). The first three points are used for the low opacity fit whereas the last seven points are used for the high opacity fit. An uncertainty of diffusive transmission around 10% is estimated from repeated measurements over an interval of several days. Also, an uncertainty around 10% is estimated for determination of opacity from the fit of coherent transmission.

results are obtained for other frequencies around the line center and also for other detection angles. Note that around the line center the incident photons are scattered close to the entrance windows corresponding to a nonequilibrium initial condition for which Eq. (3) is valid for $\alpha < 2$ [39].

IV. SIMULATIONS

In Fig. 4 we show results from Monte Carlo simulations we have performed. The Monte Carlo algorithm used is described elsewhere [40,41] and takes into account a partial frequency redistribution at each scattering event and the possibility of collisions between atoms. Three scenarios are considered for the photon scattering in atomic media. The R_{II} scenario [36,42] considers the absence of collisions between atoms and an elastic photon scattering in the atomic rest frame. This scenario is adequate for low-density vapor for which the time between collisions τ_C is longer than the excited-state lifetime τ. A fit of simulated diffuse transmission as a function of opacity using Eq. (3) gives $\alpha = 1.17 \pm 0.04$, which is consistent with the measured value [see Fig. 4(a)]. Note that for this scenario a deviation from the power law is obtained for the higher opacities as a consequence of partial correlation between absorbed and emitted frequencies in the resonance wings that makes the light transport converge to normal diffusion [36,40].

In the R_{III} scenario [36,42] collisions are very frequent ($\tau_C < \tau$) and the correlation between absorbed and emitted frequencies is lost in the atomic rest frame with the emitted frequency being redistributed in a Lorentz profile with homogeneous width $\Gamma = \Gamma_n + \Gamma_C$, with $\Gamma_n = 1/2\pi\tau = 5.2$ MHz the natural width and Γ_C the collisional width. We consider resonant dipole-dipole collisions resulting in self-broadening proportional to the atomic density [43,44] with $\Gamma_C = (9 \times 10^{-7})N$ Hz cm³ [45]. For the range of densities used in the experiment, the collisional width varies from negligible $\Gamma_C \sim$ 3 kHz for $r = 8$ to $\Gamma_C \sim 60$ MHz for $r = 1.5 \times 10^5$. In the
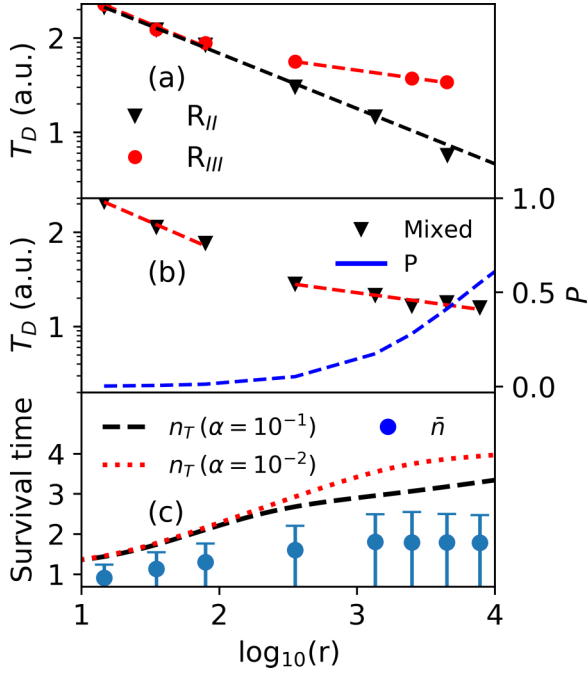
FIG. 4. (a) Simulated diffuse transmission using the Monte Carlo algorithm for the R_{II} (black triangles) and R_{III} (red circles) scenarios together with fits using Eq. (3). (b) Simulated diffuse transmission for the mixed scenario (black triangles) and probability P (blue dashed line) of a collision occurring before spontaneous emission. The values for P are shown on the right vertical axis. In (a) and (b) the uncertainty of the simulated diffusive transmission is estimated to be 5%. (c) Survival time as a function of sample opacity obtained from simulations with the mixed scenario (blue circles) together with the minimal number of scattering necessary to converge to normal diffusion calculated from Eq. (4) for $a = 10^{-1}$ (black dashed line) and $a = 10^{-2}$ (red dotted line).

laboratory frame the emitted frequency is further redistributed by Doppler broadening. The simulated diffuse transmission as a function of sample opacity exhibits a clear regime change from Doppler to Lorentz with crossover opacity similar to that observed experimentally [see Fig. 4(a)]. The obtained parameters fitting Eq. (3) were $\alpha = 1.2 \pm 0.2$ for the low-opacity regime and $\alpha = 0.40 \pm 0.02$ for the high-opacity regime.

We also considered a mixed scenario where at each scattering event we draw the probability $P = \Gamma_C/(\Gamma_n + \Gamma_C)$ [46] of occurring a collision before spontaneous emission and obtained results similar to those of the R_{III} scenario [see Fig. 4(b)]. The expected P value is also shown in Fig. 4(b). Note that the crossover from the R_{II} to the R_{III} scenario taken at $P = \frac{1}{2}$ occurs for opacities much higher than r_c, that is, the crossover from $\alpha = 1$ to $\alpha = 0.5$ observed in Figs. 3 and 4. Around the crossover opacity r_c, $\Gamma \sim \Gamma_n$ ($a = 1.1 \times 10^{-2}$) and the step-size distribution is very similar to the one calculated for $a = 10^{-2}$ [see Fig. 1(a)]. For the higher opacities used $a \sim 10^{-1}$ and a crossover to the Lorentzian regime should occur for lower opacity [see Fig. 1(a)]. Those simulation results reinforce that the crossover from the Doppler to the Lorentz regime is a truncation effect and not a change

in scattering scenario related to the emergence of collisional broadening.

From the simulations it is also possible to collect the survival time of the photons inside the sample, that is, the mean number of scattering events $\bar{n}$, which is shown in Fig. 4(c). A truncated Lévy flight converges to normal diffusion if the number of scattering events is large enough [1], with the number of steps required for the transition given by [39,47]

$$n_T = \left(\frac{5}{2}\right)^2 \left[\frac{\langle |r^3| \rangle}{\langle r^2 \rangle^{3/2}}\right]^2. \tag{4}$$

The n_T calculated for Voigt profiles with $a = 10^{-2}$ (red dotted line) and $a = 10^{-1}$ (black dashed line) are shown in Fig. 4(c) and are larger than $\bar{n}$, which justifies the observation of the Lévy flight characteristic despite truncation.

V. CONCLUSIONS

In conclusion, we have measured the dependence of the Lévy parameter α as a function of sample size for photons scattered by resonant atomic vapor. For a vapor with a Voigt absorption profile, a crossover from transport ruled by the Doppler core of the profile to one ruled by Lorentz wings was observed around an opacity of $r_c = 10^3$, resulting in a change of the parameter α from $\alpha \sim 1$ to $\alpha = 0.5$. We have evidenced that the truncation length determines the spectral region from the Voigt emission profile that contributes to the diffusion process. The observation of the crossover between the Doppler and Lorentz regimes was possible due to different experimental parameters relative to previous similar works on Lévy flights in atomic vapor. In [27] only the Lorentz regime was observed as a buffer gas was used, resulting in a large collisional width ($\Gamma_C > \Gamma_D$) and the large Voigt parameter lowering the crossover opacity $r_c < 1$. In [26] r_c was not reached in the experiment for the use of a thinner cell and of Rb vapor with larger Γ_D and a smaller Voigt parameter, compared to the Cs vapor of the present work, resulting in an increase of r_c. Note that both simulations and theory were discussed here for a two-level atom. We have not investigated the influence of the unresolved excited hyperfine structure of the Cs $6P_{3/2}$ level and suppose it can be taken into account by a larger effective Doppler width. We believe this work demonstrates that laboratory optical systems are good platforms for investigations of the random walk process and hope it can contribute to the understanding of size effects in superdiffusion.

ACKNOWLEDGMENTS

APPENDIX A: OPACITY MEASUREMENT

We have obtained sample opacity by fitting coherent transmission spectra by the Beer-Lambert law

$$T(x) = \exp\left(-\sum_i \beta_i \Phi(x - x_i) r\right), \qquad \text{(A1)}$$

with the summation over the $6S_{1/2}(F=4) \rightarrow 6P_{3/2}(F=3, 4, 5)$ transitions centered at x_i and with relative strength β_i. The $\Phi(x)$ are Voigt absorption profiles as defined in Eq. (2).

APPENDIX B: DETECTED SIGNAL TREATMENT

In the diffuse transmission spectra a signal far from resonance is detected that corresponds to light scattered at the cell output window. The spectrum shown in Fig. 2(b) was obtained by calculating

$$T_D(x) = D(x) - S(x), \qquad \text{(B1)}$$

with $D(x)$ the detected power as a function of detuning consisting of diffusive transmission plus light not absorbed by the vapor and scattered at output windows, $S(x)$. The scattered light was determined as $S(x) = \gamma P_0 T(x)$, with γ a factor taking into account the percentage of incident power P_0 that is scattered, detection efficiency, and detector gain. Here $T(x)$ is the measured vapor coherent transmission that is zero for the detuning close to the resonance and densities analyzed here.

APPENDIX C: INFLUENCE OF LASER EMISSION SPECTRA

The laser used is a diode laser with external grating cavity. That type of laser is known to possibly have low-power second-mode emission and a broad spectral pedestal that might perturb the detected signal at resonance. From the coherent transmission measurement we have verified that possible contributions of the second mode and the pedestal are less than 5% of the total beam power. This eventual nonresonant light should contribute less than 5% of $S(x)$, the scattered light at the output window. The detected signal at the line center is at least 20% (for higher opacity) of the scattered light far from resonance, which made us conclude that the eventual second mode and pedestal do not affect the measurements of diffuse transmission.

[1] R. N. Mantegna and H. E. Stanley, Phys. Rev. Lett. **73**, 2946 (1994).

[2] M. Leadbeater, V. I. Falko, and C. J. Lambert, Phys. Rev. Lett. **81**, 1274 (1998).

[3] P. Barthelemy, J. Bertolotti, and D. S. Wiersma, Nature (London) **453**, 495 (2008).

[4] N. Mercadier, W. Guerin, M. Chevrollier, and R. Kaiser, Nat. Phys. **5**, 602 (2009).

[5] A. Miron, Phys. Rev. Lett. **124**, 140601 (2020).

[6] E. M. Trotta and G. Zimbardo, Aston. Astrophys. **530**, A130 (2011).

[7] M. F. Shlesinger, B. J. West, and J. Klafter, Phys. Rev. Lett. **58**, 1100 (1987).

[8] K. Pfeilsticker, F. Erle, O. Funk, H. Veitel, and U. Platt, J. Geophys. Res.: Atmos. **103**, 11483 (1998).

[9] B. Podobnik, A. Valentinčič, D. Horvatić, and H. E. Stanley, Proc. Natl. Acad. Sci. USA **108**, 17883 (2011).

[10] S. C. Lera and D. Sornette, Phys. Rev. E **97**, 012150 (2018).

[11] S. Huda, B. Weigelin, K. Wolf, K. V. Tretiakov, K. Polev, G. Wilk, M. Iwasa, F. S. Emami, J. W. Narojczyk, M. Banaszak, S. Soh, D. Pilans, A. Vahid, M. Makurath, P. Friedl, G. G. Borisy, K. Kandere-Grzybowska, and B. A. Grzybowski, Nat. Commun. **9**, 4539 (2018).

[12] G. M. Viswanathan, V. Afanasyev, S. V. Buldyrev, E. J. Murphyt, P. Princet, and H. E. Stanley, Nature (London) **381**, 413 (1996).

[13] G. Viswanathan, E. Raposo, and M. da Luz, Phys. Life Rev. **5**, 133 (2008).

[14] B. Ríos-Uzeda, E. Brigatti, and M. V. Vieira, Sci. Rep. **9**, 2737 (2019).

[15] D. Brockmann, L. Hufnage, and T. Geisel, Nature (London) **439**, 462 (2006).

[16] M. C. González, C. A. Hidalgo, and A.-L. Barabási, Nature (London) **453**, 779 (2008).

[17] A. Reynolds, E. Ceccon, C. Baldauf, T. K. Medeiros, and O. Miramontes, PLoS One **13**, e0199099 (2018).

[18] H. Janssen, K. Oerding, F. van Wijland, and H. Hilhorst, Eur. Phys. J. B **7**, 137 (1999).

[19] C. J. Tessone, M. Cencini, and A. Torcini, Phys. Rev. Lett. **97**, 224101 (2006).

[20] T. De Ver Dye, E. Muir, L. Farovitch, S. Siddiqi, and S. Sharma, Infect. Dis. Poverty **9**, 71 (2020).

[21] B. Gross, Z. Zheng, S. Liu, X. Chen, A. Sela, J. Li, D. Li, and S. Havlin, Europhys. Lett. **131**, 58003 (2020).

[22] L. Giuggioli, G. M. Viswanathan, V. M. Kenkre, R. R. Parmenter, and T. L. Yates, Europhys. Lett. **77**, 40004 (2007).

[23] P. Barthelemy, J. Bertolotti, K. Vynck, S. Lepri, and D. S. Wiersma, Phys. Rev. E **82**, 011101 (2010).

[24] T. Svensson, K. Vynck, M. Grisi, R. Savo, M. Burresi, and D. S. Wiersma, Phys. Rev. E **87**, 022120 (2013).

[25] T. Svensson, K. Vynck, E. Adolfsson, A. Farina, A. Pifferi, and D. S. Wiersma, Phys. Rev. E **89**, 022141 (2014).

[26] Q. Baudouin, R. Pierrat, A. Eloy, E. J. Nunes-Pereira, P.-A. Cuniasse, N. Mercadier, and R. Kaiser, Phys. Rev. E **90**, 052114 (2014).

[27] M. O. Araújo, T. P. de Silans, and R. Kaiser, Phys. Rev. E **103**, L010101 (2021).

[28] R. Savo, M. Burresi, T. Svensson, K. Vynck, and D. S. Wiersma, Phys. Rev. A **90**, 023839 (2014).

[29] J. Bertolotti, K. Vynck, L. Pattelli, P. Barthelemy, S. Lepri, and D. S. Wiersma, Adv. Funct. Mater. **20**, 965 (2010).

[30] N. Mercadier, M. Chevrollier, W. Guerin, and R. Kaiser, Phys. Rev. A **87**, 063837 (2013).

[31] C. Kenty, Phys. Rev. **42**, 823 (1932).

[32] E. Pereira, J. M. G. Martinho, and M. N. Berberan-Santos, Phys. Rev. Lett. **93**, 120201 (2004).

[33] J. Weiner and P.-T. Ho, *Light-Matter Interaction: Fundamentals and Applications* (Wiley, New York, 2003).

[34] P. Siddons, C. S. Adams, and I. G. Hughes, J. Phys. B **42**, 175004 (2009).

[35] M. Chevrollier, Contemp. Phys. **53**, 227 (2012).

[36] A. R. Alves-Pereira, E. J. Nunes-Pereiraa, J. M. G. Martinho, and M. N. Berberan-Santos, J. Chem. Phys. **126**, 154505 (2007).

[37] H. Larralde, F. Leyvraz, G. Martínez-Mekler, R. Rechtman, and S. Ruffo, Phys. Rev. E **58**, 4254 (1998).

[38] S. V. Buldyrev, S. Havlin, A. Y. Kazakov, M. G. E. da Luz, E. P. Raposo, H. E. Stanley, and G. M. Viswanathan, Phys. Rev. E **64**, 041108 (2001).

[39] C. W. Groth, A. R. Akhmerov, and C. W. J. Beenakker, Phys. Rev. E **85**, 021138 (2012).

[40] J. C. d. A. Carvalho, M. Oriá, M. Chevrollier, H. L. D. d. S. Cavalcante, and T. Passerat de Silans, Phys. Rev. A **91**, 053846 (2015).

[41] J. C. de Aquino Carvalho and T. Passerat de Silans, J. Quant. Spectrosc. Radiat. Transfer **260**, 107469 (2021).

[42] D. G. Hummer, Mon. Not. R. Astron. Soc. **125**, 21 (1962).

[43] E. L. Lewis, Phys. Rep. **58**, 1 (1980).

[44] Z. Jabbour, J. Sagle, R. Namiotka, and J. Huennekens, J. Quant. Spectrosc. Radiat. Transfer **54**, 767 (1995).

[45] T. Passerat de Silans, J. Phys. B **51**, 195401 (2018).

[46] H. A. Post, Phys. Rev. A **33**, 2003 (1986).

[47] M. F. Shlesinger, Phys. Rev. Lett. **74**, 4959 (1995).